

Oxidation-induced microstructural changes of a polymer-derived Nextel™ 610 ceramic composite and impact on the mechanical performance

E. Volkmann · L. Lima Evangelista ·
K. Tushtev · D. Koch · C. Wilhelmi ·
K. Rezwani

Received: 23 April 2013 / Accepted: 18 September 2013 / Published online: 28 September 2013
© Springer Science+Business Media New York 2013

Abstract This study analyses the effects of heat treatments in oxidative atmosphere on the mechanical and microstructural properties of a fiber-reinforced weak interface composite (UMOX™) which is composed of a mullite-SiOC matrix and Nextel™ 610 fibers with fugitive coatings. Composites of different porosity grades, depending on the polymer infiltration and pyrolysis cycle, are exposed to 1000 and 1200 °C for 50 h. The exposure provokes the formation of silica, which leads to matrix densification and the formation of silica bridges at the fiber–matrix interface, resulting in an increased interfacial bonding strength. Consequently, the fracture toughness and the flexural strength are significantly reduced. The study confirms that SiOC-based materials are suitable for an application at high temperatures in oxygen-rich atmospheres up to 1000 °C. It is, however, important to consider the microstructural changes and thereby induced decrease of the overall mechanical performance during a high-temperature use.

Electronic supplementary material The online version of this article (doi:10.1007/s10853-013-7752-4) contains supplementary material, which is available to authorized users.

E. Volkmann · L. Lima Evangelista · K. Tushtev (✉) ·
K. Rezwani

Advanced Ceramics, University of Bremen, Am Biologischen
Garten 2, 28359 Bremen, Germany
e-mail: Tushtev@uni-bremen.de

D. Koch
Ceramic Composite Structures, Institute of Structures and
Design, German Aerospace Center, Stuttgart, Germany

C. Wilhelmi
EADS Innovation Works, Munich, Germany

Introduction

All-oxide ceramic matrix composites (CMCs) are promising candidates to fulfill the demand for thermostructural materials used in oxidizing atmospheres like in combustor liner of gas turbines, hot structures in re-entry vehicles or thermal insulations [1, 2]. Among the potential manufacturing routes, the polymer infiltration and pyrolysis (PIP) process could be one of the most efficient and cost-effective [3], as conventional processing routes derived from the polymer matrix field can be applied [4]. Some of the most common preceramic polymers are polysiloxanes, from which a silicon oxycarbide (SiOC) matrix can be obtained. The major drawback of this system, when compared to all-oxide matrices such as alumina, is its reactivity in oxygen-rich atmospheres. At high temperatures in air atmosphere, a parabolic oxidation rate is observed due to the formation of a passivating silica layer [5]. It is known that the oxidation of SiOC is mainly governed by two concurrent reactions: the conversion from carbon to carbon di-(oxide) and the formation of silica. Both reaction paths are influenced by the amount of free carbon, the oxidation temperature [6], the oxygen permeability [7] and pyrolysis temperature [8] of the material. Brewer et al. [6] investigated the oxidation behavior of SiOC powders with different amounts of free carbon at several oxidation temperatures. They found that with increasing content of free carbon, a complete conversion to SiO₂ is likely at 600 and 800 °C, whereas at low carbon levels and at 1000 and 1200 °C the passivating silica layer prevents the material from further oxidation. This can be explained because decreasing the amount of free carbon and increasing the oxidation temperature to 1000 or 1200 °C reduce the oxidation due to the faster passivation which hinders the oxygen entrance. Hurwitz and Meador [8] found that a

higher pyrolysis temperature of SiOC based on a commercially available preceramic resin (BlackglasTM, Allied Signal, Inc.) increased the oxidation stability of the material. This is related to an increase of SiO₄ and SiC₄ species in the material. As a consequence, other species like SiCO₃, SiC₃O or SiC₂O₂ diminish resulting in a structure with increased ordering and higher oxidation stability. Besides the material manufacturing and the oxidation conditions, the sample morphology effects the oxidation behavior of SiOC [9]. Hence, foams [10], bulk samples [11], coatings [12], powders [6, 13] and CMCs [14, 15] show different high-temperature characteristics. Considering ceramic matrix composites (CMCs), there are only very few studies of the oxidation behavior of SiOC-based composites. Gonczy and Sikona [15] investigated the behavior of a NextelTM 312/BN/BlackglasTM after oxidation at temperatures from 500 up to 700 °C for a maximum duration of 4000 h. They found that the effect on the mechanical performance depends on time and temperature. A second study was carried out by Rangarajan et al. [14] concerning the influence of the cure pressure and the pyrolysis atmosphere on the structure and performance of NextelTM 440/C/BlackglasTM composites. Exposure for 500 h at 1000 °C resulted in a higher weight loss of pyrolyzed samples in argon atmosphere when compared to samples processed in ammonium atmosphere, due to a higher amount of free carbon in the composite. However, to our knowledge, there is no study that directly investigates the impact of oxidation-induced microstructural changes on the mechanical performance.

Therefore, the aim of the present study is to analyze the changes of the microstructure of a polymer-derived composite with a fugitive coating [16]. Furthermore, these changes are expected to be related to the mechanical performance of the material after oxidation.

The investigated composite is a NextelTM 610/mullite-SiOC CMC material of EADS Innovation Works, Ottobrunn, Germany (UMOXTM). It has been developed and successfully tested for use in oxidative high-temperature environments like in gas turbine applications [17], or in thermal protection systems [18]. This material was chosen as an exemplary composite system, because a former study regarding the creep performance of an SiOC-based material with a fugitive coating implied that in combination with the SiOC-based matrix the oxidation of the material effects the interfacial bonding [19].

In this work, samples with different porosities in as-received condition and after exposure to 1000 and 1200 °C for 50 h in laboratory air environment are tested. The mechanical performance is evaluated in terms of interfacial and out-of plane strength, fracture toughness, as well as notch sensitivity. Finally, the on-axis behavior is correlated to the effects of oxidation.

Experimental

Materials

The specific type of UMOXTM used in this work has a matrix based on a commercial micron-sized mullite powder and polysiloxane precursor. Continuous alumina fibers of type NextelTM 610 were used as reinforcement fibers. A fugitive interface [16] with a thickness of approximately 40–80 nm is achieved using an organic fiber coating, which is removed by oxidative treatment after composite production. The oxide CMC is manufactured by the polymer infiltration and pyrolysis (PIP) process. Detailed information about the manufacturing of UMOXTM can be found in [17]. The pyrolysis has been accomplished in argon atmosphere at approximately 1300 °C. Shrinkage of the preceramic matrix during pyrolysis leaves porosity in the material. Therefore, up to three infiltration cycles of the composite with a polymeric precursor and high-temperature treatment are applied to reduce the open porosity. Next to the first infiltration with resin and filler particles (I1), the composite is re-infiltrated with the pure resin one (I2) or two times (I3) depending on the desired material porosity and properties (cf. Table 1). X-ray diffraction shows an increasing content of cristobalite with number of infiltrations, which can be related to the longer exposure to the processing temperature.

Preparation of specimens and heat treatment

The specimens for the mechanical tests were cut using a diamond disc precision cutter CUTO 1 (Jean Wirtz, Düsseldorf, Germany) with a diamond-coated disc rotating at 1000 rpm. The notches for the SENB samples were prepared with a diamond wire saw WellTM 6234 (Well, Mannheim, Germany) with a wire of 0.5 mm in thickness and using a linear cutting speed of 1.0 m/s. The heat treatment of all samples was accomplished with an HT 40/17 oven (Nabertherm, Lilienthal, Germany) at 1000 and 1200 °C for 50 h. The time corresponds to over 90 % of the maximum mass gain at 1000 °C, which is reached in a furnace after approximately 250 h. A heating rate of 10 K/min was used. Before oxidizing, sintering rings with a temperature range of 970–1250 °C (Ferro electronic material systems, Uden, Netherlands) were used to verify the spatial heat distribution homogeneity of the furnace.

Physical and structural characterization

The open porosity of the samples was determined with the Archimedes method according to DIN EN 623-2. The total porosity was calculated with the help of Helium

Table 1 Overview of the used UMOXTM materials

ID	Layup	Matrix	Infiltrations	Fiber	Open porosity in %	Total porosity in %
I1	16 layers: [0/90] _s cross ply	Mullite + SiOC	1	Nextel TM 610 99 %	26.2 ± 0.8	22.6 ± 1.4
I2			2	α-Al ₂ O ₃ 48–50 Vol. %	16.12 ± 0.9	17 ± 0.6
I3			3		11.94 ± 0.33	11.9 ± 0.5

pycnometry in an AccuPyc 1330 (Micromeretic, Norcross, US). To investigate a potential size effect, the open porosities of all tested dimensions were determined and compared.

Mechanical testing

Through thickness tensile test (TTT)

The through thickness tensile test was performed using a Zwick/Roell Z005 (Zwick, Ulm, Germany) universal testing machine with a 5 kN HBM U2B load cell (HBM, Darmstadt, Germany). The crosshead displacement rate was 0.5 mm/min. To minimize possible edge effects [20], the preparation of the 10 mm × 10 mm specimens was accomplished with a diamond disc precision cutter CUTO 1 (Jean Wirtz, Düsseldorf, Germany). The samples were glued on steel screws with a diameter of 3.5 mm. An ambient curing epoxy resin UHU Plus Schnellfest (UHU GmbH & Co. KG, Bühl/Baden, Germany) was used and cured at room temperature to prevent thermal stresses [20]. During the 30-min curing time the machine was set to a constant load of 10 N pressure to avoid tensile stresses on the sample. Before that, the screws were ground to assure a flat surface for gluing the sample on it. At least 8 samples per material were tested.

Push-in test

The push-in test [21] was used to determine the bonding strength between fiber and matrix. A Vickers-type indenter was used in a load–unload–reload–unload cycle up to a maximum load of 0.6 N. 30 fibers per sample were tested.

Single edge-notched bend test (SENB) and four-point bending test (4 PB)

The dimension of the SENB samples was 70 mm × 10 mm with a 3-mm notch. The depth of the notch was measured with a digital optical microscope VHX-600 (Keyence, Frankfurt, Germany) at a magnification of 50×. The dimension of the 4 PB samples was 70 mm × 7 mm. It was chosen with respect to the residual cross section of the SENB samples. The bending test was

accomplished according to DIN EN 658-3 with loading in edge direction of the samples to allow a direct comparison with the SENB test. As can be seen the CMC shows a substantial linear behavior which allows a calculation of the flexural strength of the composite. For both tests, five samples per composite were tested in the same machine/loadcell combination as used for the TTT. The crosshead displacement rate was 0.5 mm/min. A four-point bending setup was used with a distance of 20 and 60 mm between the upper and the lower noses, respectively.

The SENB test is well established for the examination of the fracture toughness of ceramic matrix composites [22, 23]. The formal fracture toughness was calculated by [24]:

$$K_{Ic} = \frac{F_{max}}{B\sqrt{W}} \frac{S_1 - S_2}{W} \frac{3\Gamma_M\sqrt{\alpha}}{2(1-\alpha)^{3/2}} \quad (1)$$

$$\Gamma_M = 1.1215\sqrt{\pi} \left[\frac{5}{8} - \frac{5}{12}\alpha + \frac{1}{8}\alpha^2 + 5\alpha^2 + 5\alpha^2\beta^6 + \frac{3}{8}\exp\left(-6.1342\frac{\alpha}{\beta}\right) \right] \quad (2)$$

where B and W are, respectively, the thickness and the height of the specimen in mm, c is the notch length in mm, S_1 and S_2 are the distances of the inner and loading span also in mm, α is the relative crack length (c/W) and β is equal to $1 - \alpha$. The single edge-notched beam test is based on the assumption of linear elastic mechanics. Therefore, and because the calculation is based on the length of the artificial notch, the calculated fracture toughness is not the real, but a formal one.

In addition, the relative work of fracture was calculated by integration of the force–displacement curve and dividing it by the residual cross sectional area of the notched sample. It should be noted that calculated values of the relative work of fracture should only be seen as reference point because they are not based on the real sample deflection due to the use of a four-point bending set up.

Statistical analysis

The statistical analysis was performed using the statistical software Minitab 16.1.1 (Minitab Inc., State College, US). To compare distinct infiltration steps before and after heat treatment at 1000 °C for 50 h, a Student's t test was used. Before that, the normality of the data and equality of the

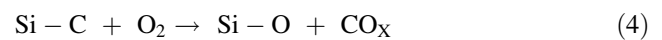
variances were checked with an Anderson–Darling and an F Test, respectively. To investigate the influence of the two heat treatments on the I3 composite, a one-way analysis of variance (ANOVA) with post hoc Tukey’s multiple comparison method was used. For all tests a p value of $p < 0.05$ was considered as statistically significant.

Results and discussion

Physical and structural characterization

The porosity of polymer derived CMCs is related to the formation of shrinkage cracks and the density change of the matrix material, due to the pyrolysis of the polymer matrix. In UMOXTM, the amount of matrix shrinkage and porosity is reduced with the help of mullite particles, acting as inert filler. The number of cracks and the amount of additional porosity generated during the pyrolysis are reduced by up to two re-infiltrations. The partial closing of the cracks and the filling of porosity lead to a densification of the composite (cf. Table 1). As depicted in Fig. 1, the cracks in the outer layers are reduced after two re-infiltrations, whereas the cracks in the middle layers remain more open. The symmetrical 0°/90° stacking sequence with 16 layers leads to a double layer with the same fiber orientation in the center of the sample. Hence, the cracks in the middle of the sample are wider and cannot

be completely filled. Besides the reduction of porosity, the additional matrix causes a change of the material’s color due to the increasing carbon content in the material (cf. Fig. 2). For the standard material (I3) this could be determined with the help of a combustion analysis to approx. 1.3 mass % carbon. Furthermore, the oxidation of the material is accompanied by a change of its color. Whereas the increasing carbon content leads to a darker material, the oxidation leads to a brighter color of the whole composite. Hence, we suppose that oxygen ingress is assured for all samples and the reactions are only limited by the amount and accessibility of carbon in the composites. Apart from the color of the sample, the heat treatment caused a gain in weight that is also found for SiC [25] and SiOC fibers [7]. As mentioned earlier, the oxidation of SiOC is governed by two main reactions [6]:



While the first reaction is accompanied by a net weight loss, the second one causes a net gain in weight. Supplementary figure A1 depicts thermogravimetric analysis for I3 in the temperature range from room temperature to 1000 °C. After an initial weight loss due to the removal of organic contaminants and water, a nearly stable temperature region was observed at 300–500 °C. Above 500 °C a slight decrease of the mass was found up to approximately 800 °C. Further increase in temperature

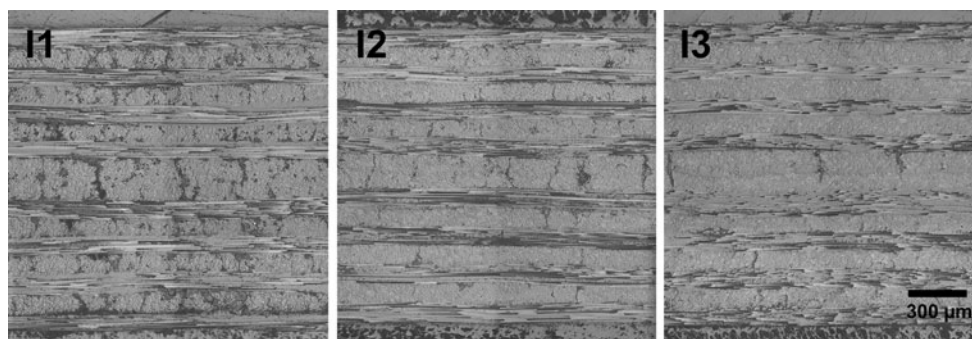


Fig. 1 Microstructure of UMOXTM with different infiltration steps showing shrinkage cracks and the cross ply layup

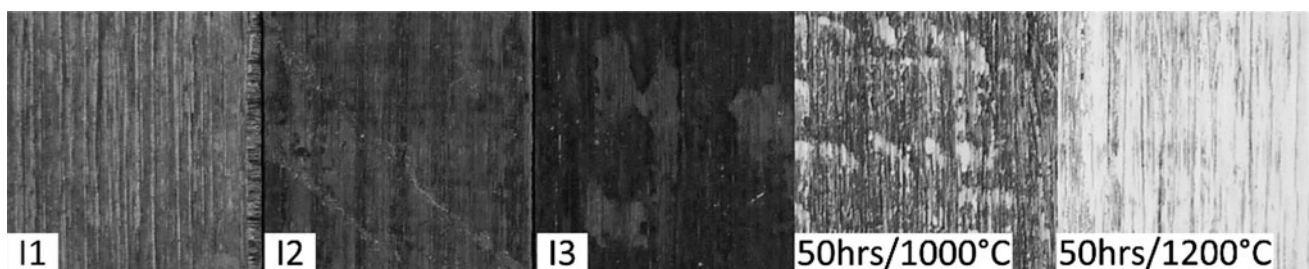


Fig. 2 Comparison of the color (*gray scale images*) of the tested materials for different infiltration steps and change of the surface color of the materials after heat treatment for I3. All pictures were taken with equal camera settings

resulted in a slight mass gain. Because of the high pyrolysis temperature and the low carbon content of the material, the weight loss due to reaction (3) is lower compared to the gain according to reaction (4). Thus, a net gain in weight is generally observed. The formation of cristobalite as a result of this reaction was identified by X-ray diffraction. As it can be seen in Fig. 3, the increase in weight is related to the infiltration step and the temperature. The bars show the average and the standard deviation of all geometries, varying from 5 mm × 5 mm (STA) up to 70 mm × 10 mm (SENB). This was done because no difference of the relative mass gain was found between the geometries within the investigated time intervals, which may be explained by the easier entrance of the oxygen through the shrinkage cracks and the gaps between fiber and matrix. For the treatment at 1000 °C, the mass gain significantly increases from 0.26 ± 0.05 % for the I1 material to 0.5 ± 0.03 and 0.6 ± 0.08 % for the I2 and the I3 material, respectively. This might be explained by the increasing amount of SiOC. In contrast to the first infiltration step of the material, the re-infiltrations are done without filler particles. Therefore, each re-infiltration cycle will lead to a higher amount of SiOC in the material. To investigate the effect of the temperature, the standard composite (I3) was also exposed to 1200 °C where an increase of the samples' mass up to 0.76 ± 0.03 % is found related to the higher oxidation rate. In combination with the reduction of the open porosity as depicted in Fig. 4, it can be concluded that the heat treatment of the samples causes the formation of a silica layer on the accessible surfaces of the substrate. Besides the surface of the micro cracks, also the gap between fiber and matrix represents a possible oxidation site.

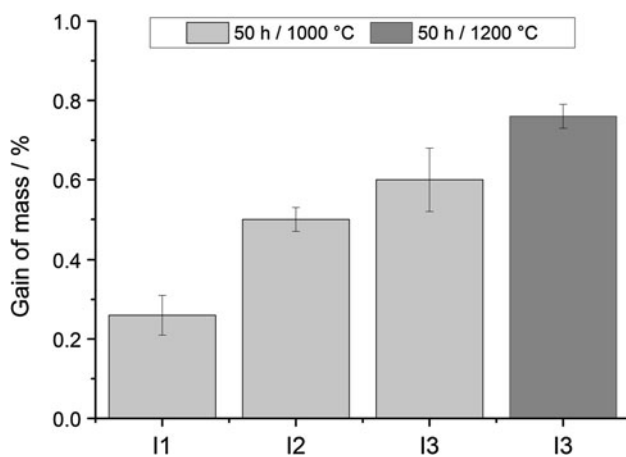


Fig. 3 Gain of mass during heat treatment for 50 h at 1,000 and 1,200 °C, respectively. At least 25 samples of different geometries were measured. All differences are significantly analyzed by a one-way ANOVA combined with Tukey's multiple comparison test at a significance level of $\alpha = 0.05$

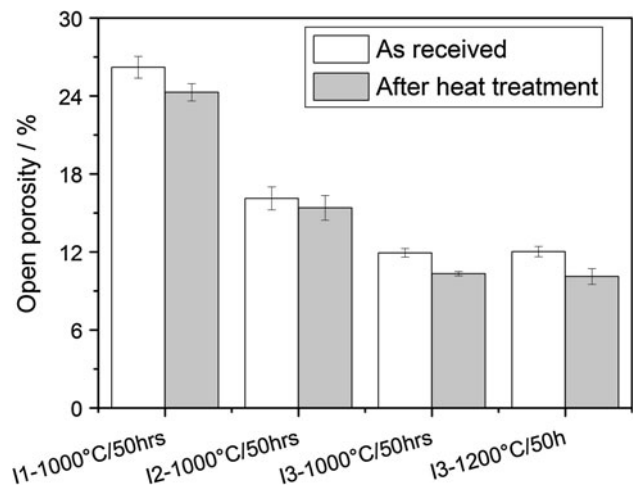


Fig. 4 Open porosity before and after heat treatment. The values present a significant difference between as-received samples and after heat treatment (One-tailed t test $\alpha = 0.05$)

Mechanical testing

Through thickness tensile test and push-in test

In the tested materials the fracture toughness is mainly provided by the gap between fiber and matrix due to the removal of the fugitive coating. The oxidation of the matrix material and the gap between fiber and matrix as potential oxidation site pose the question of the influence of silica formation on the mechanical properties.

The through thickness tensile test is used to investigate the out-of-plane strength of the material. The fracture surface of the different materials showed fracture through different layers, cf. Figure 5. Fiber–matrix interface debonding, as well as matrix fracture zones was visible, because the crack travelled through different plies of the sample. This might be related to the lack of a matrix-rich interface between the layers, the biphasic matrix and the shrinkage cracks in the midplane of the composites. Whereas the porous SiOC network and the shrinkage cracks (cf. Fig. 1) will only provide a small resistance against crack propagation, the dense mullite particles and the fibers may cause crack deflection. The ratio of crack deflection in the matrix and in the interface is depending on the porosity in the SiOC matrix. Hence, compared to the I3 composite, the material with only one infiltration showed slightly more matrix fracture zones, due to the weaker matrix. The through thickness tensile strength of the materials before and after the heat treatment is shown in Fig. 5. The strength increased significantly from 1.8 ± 0.5 MPa for I1 to 5.1 ± 0.8 MPa for I3. The heat treatment caused an additional significant increase for I1 and I2 at 1000 °C and for the I3 material for 1200 °C.

While the TTT measures the combined strength of the matrix and the interface, the push-in test determines only the properties of the interface. To identify a displacement of the fiber after the push-in test, profilometer measurements were performed. As shown in Fig. 6a, the interfacial

fracture behavior changes after the heat treatment. Before the heat treatment, the fiber can be detached from the surrounding matrix, while after the heat treatment no debonding could be achieved (cf. Fig. 6b). This could be verified in the push-in curves. Typical push-in curves for

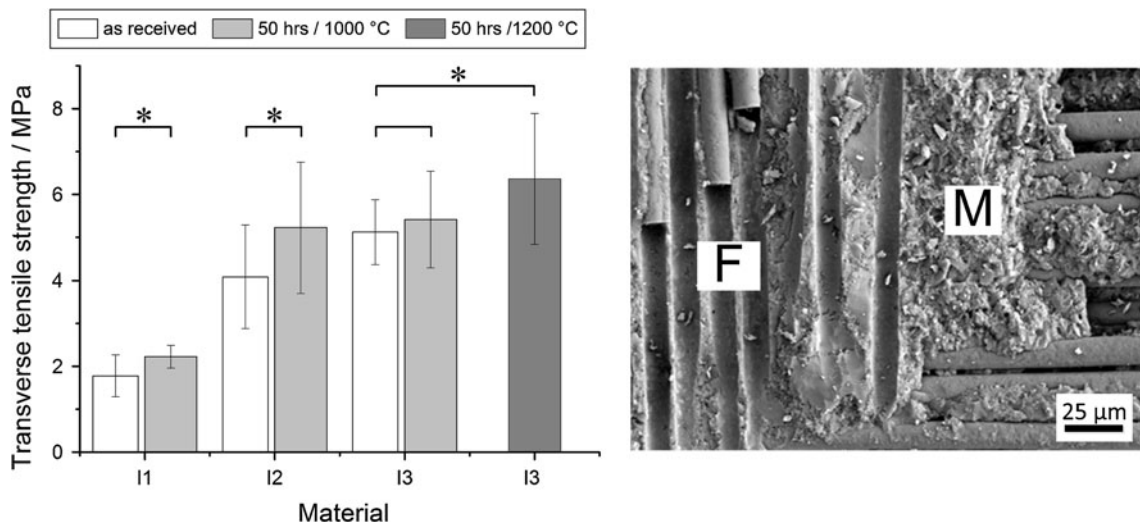


Fig. 5 Left Influence of infiltration and oxidation on the transverse tensile strength of UMOXTM. Brackets identify the datasets compared by a one-tailed *t* test ($\alpha = 0.05$). Significant differences are marked

with an *asterisk*. Right Representative fracture surface after transverse tensile test. Sample with two infiltrations (I3); *M* labels a matrix fracture zone and *F* labels an interface fracture zone, respectively

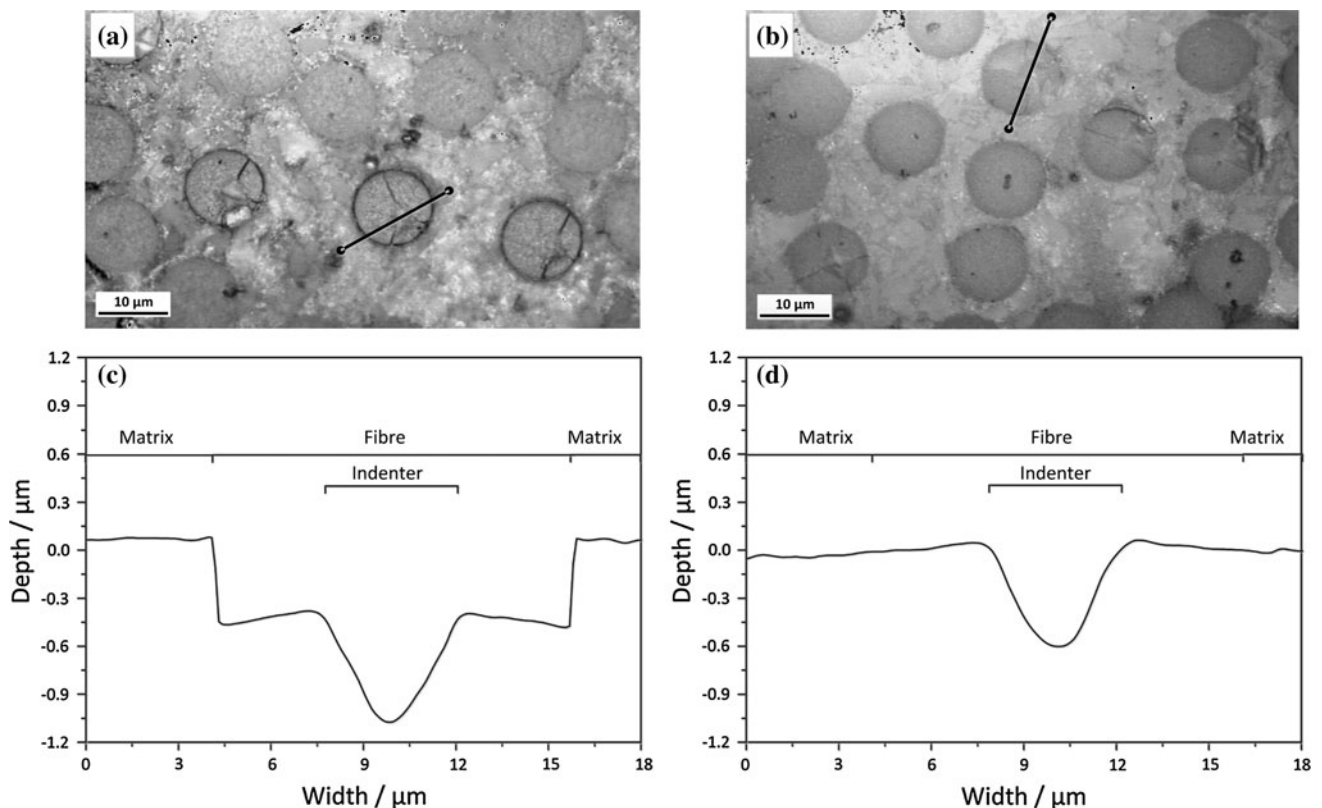


Fig. 6 Microsections (a, b) and profilometer measurements (c, d) of a pushed fiber in an as-received I3 (left) and a sample after 50 h at 1200 °C (right). The black lines in a and b show the measurement path

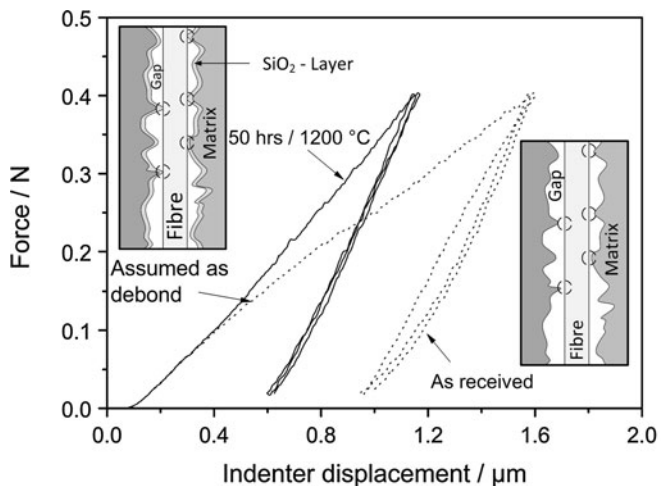
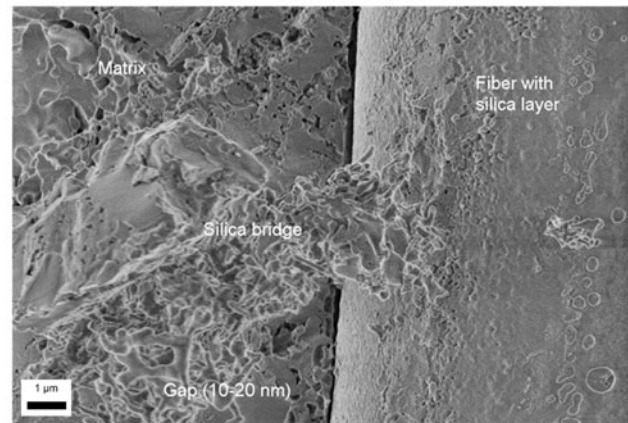


Fig. 7 *Left* Typical Push-in curves for I3 as-received and heat-treated samples. The simplified schematic *insets* show a possible effect of the formation of a silica layer on the mullite-SiOC matrix. The *dashed circles* show possible connections between fiber and matrix. *Right*



SEM image of a fracture surface after transverse tensile test (I3, 1200 °C/50 h) showing a silica bridge emanating from the SiOC matrix. Magnification: 20 k; Working distance: 1.9 mm; 0.5 kV; SE InLens detector

the I3 material before and after heat treatment at 1200 °C for 50 h can be seen in Fig. 7. After the heat treatment, the material showed nearly linear force–displacement behavior and a closed hysteresis loop, which is related to the strong bonding between fiber and matrix. In contrast, the slope of the as-received material decreased at approximately 0.15 N and shows an open hysteresis loop, possibly caused by the reduced frictional stresses in the interface as a result of the partial debonding.

However, for all samples fiber fracture is found after the test, probably due to the sharp edges of the Vickers indenter. Hence, it is difficult to state whether the fiber fracture or the debonding happened first. When considering the profilometer measurements (Fig. 6), it may be assumed that fiber fracture has no considerable influence on the general shape of the force–displacement curves (Fig. 7). In any case it can be stated that without heat treatment all fibers could be pushed in with 0.4 N, whereas for the material exposed to 1000 °C, only 63 % could be pushed and for the material exposed to 1200 °C no fiber could be debonded even at 0.6 N.

A fugitive coating provides a gap between fiber and matrix. Hence, no tensile loads can be carried in the transverse direction, while in fiber direction, the friction in the interface is a result of the topological interlocking of fiber and matrix asperities. However, transverse tensile and push-in tests show that the transverse tensile and the interfacial shear strength are increased after oxidation. A possible explanation is given in the insets in Fig. 7 (left). Prior to the heat treatment the gap between fiber and matrix features a low friction and, theoretically, no direct connections in the interface. As

mentioned earlier the heat treatment of the composite induces a silica layer formation, which is schematically shown in Fig. 7. The newly formed layer on the SiOC in combination with the roughness of fiber and matrix leads to direct connections between the two components. The existence of silica bridges is confirmed by SEM analysis depicted in Fig. 7 (right). While the basic interfacial gap is still present, several silica bridges arose from the SiOC in the matrix.

In general, the strength of ceramics is strongly dependent on the porosity of the material, i.e. of the matrix in case of CMC. It is thus important to know if the transverse tensile strength of the tested CMCs is not only affected by the porosity of the matrix but is also influenced by the interfacial bridges between fibers and matrix.

For the as-received material, with no bridges, the strength shows a rather constant decrease with increasing porosity. In contrast, no clear trend could be observed for the oxidized material. For example, the through thickness tensile strength for the I3 material increased by approximately 6 % after 50 h at 1000 °C and it increased by 24 % for the material oxidized for 50 h at 1200 °C compared to the as-received condition. However, the porosity is reduced by 14 % for the treatment at 1000 °C, but for the exposure at 1200 °C it decreased only by further 2 %, which is a clear indication that the reduction of the matrix porosity is not the only factor affecting the through thickness tensile strength.

In summary, the formations of the bridges increase the interfacial strength of the material and, in combination with the general densification of the matrix, they enhance the through thickness tensile strength.

Single edge-notched bend and flexural test

The change of the open porosity and the interfacial properties after oxidation points to the question of the on-axis strength and notch sensitivity of the material. The flexural test of the material shows a constant linear slope up to a maximum load independent of the material state, followed by a sudden fracture. In the SENB test, only samples exposed to 1200 °C tend to a brittle failure after the initial linear slope, whereas the other material states show a graceful failure (cf. Fig. 8). In contrast to the stiffness, the heat treatment of the material decreases strength in both setups. The embrittlement of the material leads to a reduction of the area under the curve that is directly related to the relative work of fracture, which decreases from 3 ± 0.3 , to 1.2 ± 0.2 , and 0.3 ± 0.03 Nmm/mm² for the as-received, the 50 h/1000 °C, and the 50 h/1200 °C state, respectively. Also the fracture toughness decreases significantly from 7.7 ± 0.04 , to 6.1 ± 0.57 , and 3.6 ± 0.14 MPam^{-0.5} for

the as-received, the 50 h/1000 °C, and the 50 h/1200 °C state, respectively, (cf. Fig. 9). As it can be seen the decrease of the relative work of fracture is more pronounced than the reduction in fracture toughness. This might be explained because it is related to the fracture progress after the onset of unstable crack growth, which is induced by debonding, fiber bridging and pullout. However, besides the changes in the interface and the matrix, the exposure at 1200 °C influenced the Nextel™ 610 fiber grain size as depicted in Supplementary A2. A tendency to grain coarsening was observed after the heat treatment (cf. Figure A2). Schmücker et al. [26] reported after only one hour exposure time, grain coarsening for Nextel™ 610 fibers, decreasing their tensile strength. The superposed effect of the fiber strength degradation and the increasing notch sensitivity of the material due to oxidation effects can be also seen by the direct comparison of the SENB and 4 PB strength (cf. Figure 9). It should be noted that the SENB and the 4 PB samples had the same net section. However, after the exposure at 1000 °C,

Fig. 8 *Left* Representative stress—crosshead displacement curves for the SENB test after different heat treatments. *Right* Comparison of the crack path of an as-received and a heat-treated sample (I3)

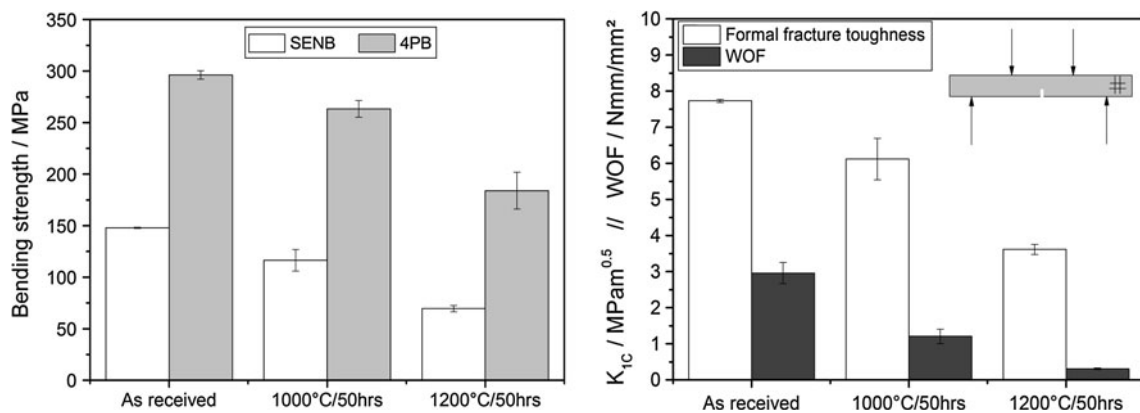
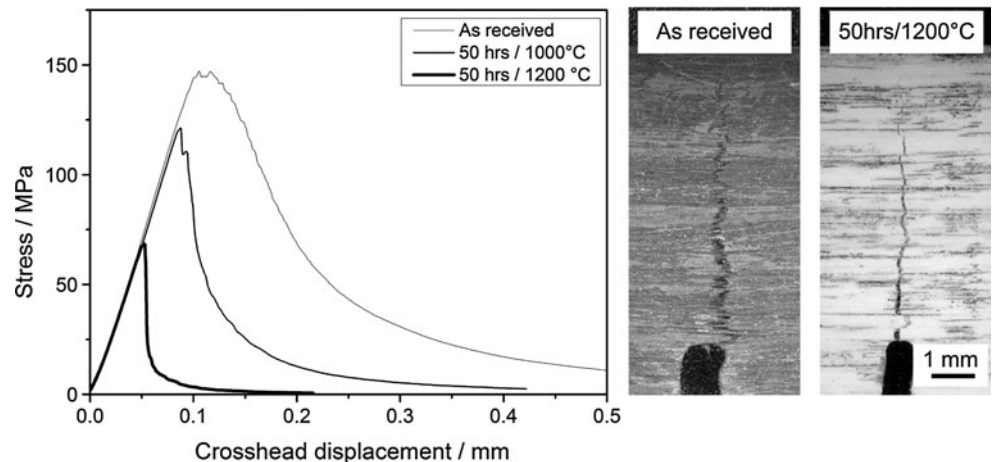


Fig. 9 *Left* Comparison of flexural strength calculated from the four-point bending test and the SENB test. For the strength of the SENB samples the residual cross section was used. All differences are significant analyzed by a one-way ANOVA combined with Tukey’s multiple comparison test at a significance level of $\alpha = 0.05$. *Right*

Comparison of fracture toughness based on the SENB test and relative work of fracture. All differences are significant analyzed by a one-way ANOVA combined with Tukey’s multiple comparison test at a significance level of $\alpha = 0.05$

the strength decreases only by 11 % for the bending tests and by 21 % for the SENB test, but it decreases by 38 and 52 % after exposure at 1200 °C for the bend and the SENB test, respectively. The effect of matrix oxidation can be seen in the reduction of the relative strength of the SENB to the 4 PB test, as this is a direct indication for the notch sensitivity of the material. This should not be influenced by the fiber strength, because all samples at one temperature level were exposed together and therefore the strength reduction is assumed to be comparable.

Conclusion

The oxidation of UMOXTM increases the through thickness tensile strength, due to a densification of the matrix accompanied by an increase of the fiber–matrix adhesion, resulting in a reduction of fracture toughness and bending strength. In contrast, the stiffness of the material is not affected by the heat treatments.

The change of the composite composition after oxidative exposure at high temperature can be measured in terms of porosity decrease, net gain in weight and change of the surface color of the material. Hereby, a higher amount of SiOC leads to a higher mass increase and better out-of-plane performance. Temperature treatment of the I3 material at 1200 °C, which is approximately 50–100 °C above the maximum allowed operation temperature of the composite, results in a significant increase of the transverse tensile strength of 24 %. The enhanced transverse and interfacial adhesion in combination with coarsening of the NextelTM 610 fibers significantly decrease the fracture toughness, and a decrease of the bend strength of 52 and 38 %, respectively. However, exposure at 1000 °C only leads to a slight increase of the through thickness and interfacial adhesion but has no effect on the reinforcement phase. The resulting reduction of the fracture toughness and flexural strength is 21 and 11 %, respectively.

The study shows that the effects of high temperatures in oxidizing atmospheres have to be taken into account when designing SiOC-based composites components with a fugitive interface for long-term applications. In combination with NextelTM 610 fibers, an operation temperature of 1200 °C or above is critical, due to the structural changes in the fiber. Whereas the stiffness of the materials is not affected, the strength of the materials is significantly decreased during exposure. However, considering the manufacturer's allowables and changes in the material, SiOC-based composites can still be promising candidates for the use in oxidizing atmospheres depending on the desired application and the resulting loadcase.

Acknowledgements The authors would like to thank T. Machry from EADS Innovation Works for the support during the manufacturing of the materials and P. Witte of Historische Geologie–Paläontologie, University Bremen for the help with the SEM pictures. Fruitful discussions with T. C. Schumacher from University of Bremen are gratefully acknowledged.

References

- Zok FW (2006) *J Am Ceram Soc* 89(11):3309–3324
- Knoche R, Werth E, Weth M, García JG, Wilhelmi C, Gerendás M (2011) In: *Mechanical properties and performance of engineering ceramics and composites VI*. Wiley, pp 77–87. doi: [10.1002/9781118095355.ch7](https://doi.org/10.1002/9781118095355.ch7)
- Motz G, Schmidt S, Beyer S (2008) *The PIP-process: precursor properties and applications*. Ceramic matrix composites. Wiley, New York
- Jones R, Zweda A, Petrak D (1999) *Compos A Appl Sci Manuf* 30(4):569–575. doi: [10.1016/s1359-835x\(98\)00151-1](https://doi.org/10.1016/s1359-835x(98)00151-1)
- Modena S, Soraru GD, Blum Y, Raj R (2005) *J Am Ceram Soc* 88(2):339–345. doi: [10.1111/j.1551-2916.2005.00043.x](https://doi.org/10.1111/j.1551-2916.2005.00043.x)
- Brewer CM, Bujalski DR, Parent VE, Su K, Zank GA (1999) *J Sol Gel Sci Technol* 14(1):49–68. doi: [10.1023/a:1008723813991](https://doi.org/10.1023/a:1008723813991)
- Chollon G (2000) *J Eur Ceram Soc* 20(12):1959–1974. doi: [10.1016/s0955-2219\(00\)00101-1](https://doi.org/10.1016/s0955-2219(00)00101-1)
- Hurwitz FI, Meador MAB (1999) *J Sol Gel Sci Technol* 14(1):75–86. doi: [10.1023/a:1008727914900](https://doi.org/10.1023/a:1008727914900)
- Soraru GD, Suttor D (1999) *J Sol Gel Sci Technol* 14(1):69–74
- Takahashi T, Münstedt H, Modesti M, Colombo P (2001) *J Eur Ceram Soc* 21(16):2821–2828. doi: [10.1016/s0955-2219\(01\)00220-5](https://doi.org/10.1016/s0955-2219(01)00220-5)
- Xu TH, Ma QS, Chen ZH (2011) *Ceram Int* 37(7):2555–2559. doi: [10.1016/j.ceramint.2011.03.053](https://doi.org/10.1016/j.ceramint.2011.03.053)
- Harris M, Chaudhary T, Drzal L, Laine RM (1995) *Mater Sci Eng A* 195:223–236. doi: [10.1016/0921-5093\(94\)06522-5](https://doi.org/10.1016/0921-5093(94)06522-5)
- Wang Y, Li H, Zhang L, Cheng L (2009) *Ceram Int* 35(3):1129–1132. doi: [10.1016/j.ceramint.2008.05.006](https://doi.org/10.1016/j.ceramint.2008.05.006)
- Rangarajan S, Belardinelli R, Aswath PB (1999) *J Mater Sci* 34(3):515–533. doi: [10.1023/a:1004590527954](https://doi.org/10.1023/a:1004590527954)
- Gonczy ST, Sikonia JG (2005) In: Bansal NP (ed) *Handbook of ceramic composites*. Springer, pp 347–373. doi: [10.1007/0-387-23986-3_15](https://doi.org/10.1007/0-387-23986-3_15)
- Weaver JH, Yang J, Zok FW (2008) *J Am Ceram Soc* 91(12):4003–4008. doi: [10.1111/j.1551-2916.2008.02746.x](https://doi.org/10.1111/j.1551-2916.2008.02746.x)
- Gerendás M, Cadoret Y, Wilhelmi C, Machry T, Knoche R, Behrendt T, Aumeier T, Denis S, Göring J, Koch D, Tushev K (2011) In: *ASME Turbo Expo 2011, Vancouver, 06-10-Juni 2011*. ASME, p 45460
- Fischer WP, Ritter H (2012) In: *42nd International Conference on Environmental Systems*. International Conference on Environmental Systems (ICES). American Institute of Aeronautics and Astronautics. doi: [10.2514/6.2012-3518](https://doi.org/10.2514/6.2012-3518)
- Casas L, Martinez-Esnaola JM (2004) *Mater Sci Eng Struct Mater Prop Microstruct Process* 368(1–2):139–144. doi: [10.1016/j.msea.2003.11.014](https://doi.org/10.1016/j.msea.2003.11.014)
- Weaver JH, Yang J, Evans AG, Zok FW (2008) *Compos Sci Technol* 68(1):10–16
- Kuntz M, Grathwohl G (2001) *Adv Eng Mater* 3(6):371–379. doi: [10.1002/1527-2648\(200106\)3:6<371:aid-adem371>3.0.co;2-y](https://doi.org/10.1002/1527-2648(200106)3:6<371:aid-adem371>3.0.co;2-y)
- Kuntz M (1996) *Rißwiderstand keramischer Faserverbundwerkstoffe*. Berichte aus der Werkstofftechnik. Shaker, Aachen
- Zok F, Sbaizero O, Hom CL, Evans AG (1991) Mode I fracture resistance of a laminated fiber-reinforced ceramic. *J Am Ceram Soc* 74(1):187–193. doi: [10.1111/j.1151-2916.1991.tb07316.x](https://doi.org/10.1111/j.1151-2916.1991.tb07316.x)

24. Munz D, Fett T (1999) *Ceramics—mechanical properties, failure behaviour, materials selection*, vol B 125. Springer, Berlin Heidelberg New York Tokyo
25. Presser V, Nickel KG (2008) *Crit Rev Solid State Mater Sci* 33(1):1–99. doi:[10.1080/10408430701718914](https://doi.org/10.1080/10408430701718914)
26. Schmücker M, Flucht F, Schneider H (2001) In: Krenkel W, Naslain R, Schneider H (eds) *High temperature ceramic matrix composites*. Wiley, Weinheim, pp 73–78